



Research article


UDC 531

DOI: 10.34910/MCE.117.13



Elliptical underground concrete block bridge with minimal weight

Yu. Ya. Tyukalov  
Vyatka State University

 yutvgu@mail.ru

Keywords: arch bridge, finite element method, concrete blocks, optimal parameters, possible displacements principle

Abstract. An algorithm for determining the optimal parameters of an elliptical road bridge made of concrete blocks is proposed. The arch section heights are determined from the condition that the height of the concrete compressed zone should not be less than half the section height at any position of the automobile load. To solve the problem by the finite element method in physically nonlinear formulation, the principle of possible stress states is used. The nodes equilibrium equations of the arch are compiled using the possible displacements principle. The arch internal forces by a finite element length are approximated with linear functions, the concrete deformation diagram is represented in a piecewise-broken curve. Also, to determine the bearing capacity reserve of the optimal arch, the arch calculations were performed with a gradual increase in the automobile load up to destruction. Three options for the vehicle load location were considered. The optimal parameters of an arched road bridge with a span of 12 meters and its bearing capacity have been determined. It is shown that the arch destruction occurs with an increase in the load from the car by about 1.6 times.

Citation: Tyukalov, Yu.Ya. Elliptical underground concrete block bridge with minimal weight. Magazine of Civil Engineering. 2023. 117(1). Article no. 11713. DOI: 10.34910/MCE.117.13

1. Introduction

Arched concrete and reinforced concrete structures with soil backfill are widely used for bridge crossings and overpasses. Such constructs are easy to manufacture and economical. The article [1] proposes an analytical method for determining the internal forces of arched lintels. Elastoplastic work of the arch material is considered. Three differential equations of equilibrium are solved analytically, and an example of calculating an arch for a concentrated force action is given. In [2], a model of cracking and plastic deformation of reinforced concrete arches is considered. The solution was obtained based on the additional energy functional and the generalized criterion for the propagation of the Griffith's crack. Comparison of numerical solutions with an experimental data is carried out. In articles [3], [4] numerical and experimental studies of brick arches are given. In [3], an arch is represented by a rigid blocks system connected by three links. The study used combinatorial analysis to determine the hinges position at small supports displacements. The article [5] investigates the mechanisms of a stone vaults destruction under the concentrated forces action. There is noted the importance of considering the of occurrence displacements possibility between rigid blocks.

Several articles are devoted to the optimization of the arches shape [6, 7]. The article [6] optimizes the shape of an underground concrete arch to reduce bending stresses. The arch is calculated using a nonlinear finite element model. The arch center line approximated by the Bezier curve with three freedom degrees. The optimal parameters are determined using a genetic algorithm. The mechanisms of stone arches destruction and concrete blocks arches are very similar. The articles [8–11] are devoted to the masonry arched bridges. The article [12] provides an overview of studies on the methods of reinforcing

brick arches with composite materials. In particular, the use of fiber cement matrix (FRCM) materials for reinforcing brick arches is investigated in [13]. The article presents numerical and experimental studies of arches reinforced with such materials. Arches are modeled using a set of rigid blocks. In a few works, volumetric finite elements are used for calculating stone and concrete structures [11, 14, 15]. In [11], the application of the combined finite discrete element method (FDEM) for the analysis of three-dimensional stone structures from dry stone is presented. The article [16] presents the results of experimental and numerical studies of the response of a multi-span arched masonry bridge by vertical static loads. In [17], a two-phase strategy for the numerical simulation of the stone destruction process of arched bridges is presented. The stone blocks are represented by solid elements, and the solution is described by special finite elements. Three modes of destruction (compression, tension, shear) of masonry materials are considered. Article [18] is devoted to the numerical analysis of masonry, based on experimental data. When calculating arched bridges, it is important to consider shear deformations. The theory of shear deformations accounting of the circular arches was proposed in [20]. This article presents an analytical solution for calculating circular arches, based on the use of logarithmic functions. Consideration of shear deformations based on stress approximations is presented in [19, 20]. In [21], an algorithm for determining the optimal dimensions of swept arches from concrete blocks is presented. To solve a physically nonlinear problem, the functional of additional energy is used in combination with the possible displacement principle [22, 23]. Internal forces along the length of a finite element are approximated by piecewise constant functions. The discrete element method has been successfully used to calculate stone arches considering nonlinearity [24-27]. Considerable attention is paid to considering the influence of such factors as rain, displacement of supports, shock loads on the strength and stability of arched structures [28-30].

The purpose of this work is to build an algorithm for finding the optimal dimensions of an arched elliptical bridge made of concrete blocks. With a given bridge span and a given minimum section height, it is required to determine the arch height and the section height change along the arch length, ensuring the minimum arch weight under the design loads action.

The solution of a physically nonlinear problem is based on the principles of possible stress states and possible displacements. Internal forces are approximated by linear functions, a concrete deformation diagram is represented in a piecewise-broken curve.

2. Methods

The arch concrete blocks are deformed together, and the nodes remain rigid, due to the joints compression by the longitudinal forces that arise in the arch systems, and due to the friction forces, that act at the junction between the blocks (Fig. 1). The absence of shear translation between the blocks is ensured by the friction forces of concrete against concrete in the compressed zone. Therefore, the required arch section height will be determined from the condition of concrete strength, as well as from the condition of ensuring the compressed zone height is not less than half of the section. In calculation process, the section shear strength will be tested against the transverse force action that occurs in the section (30). Therefore, in the finite element scheme, the nodes are assumed to be rigid.

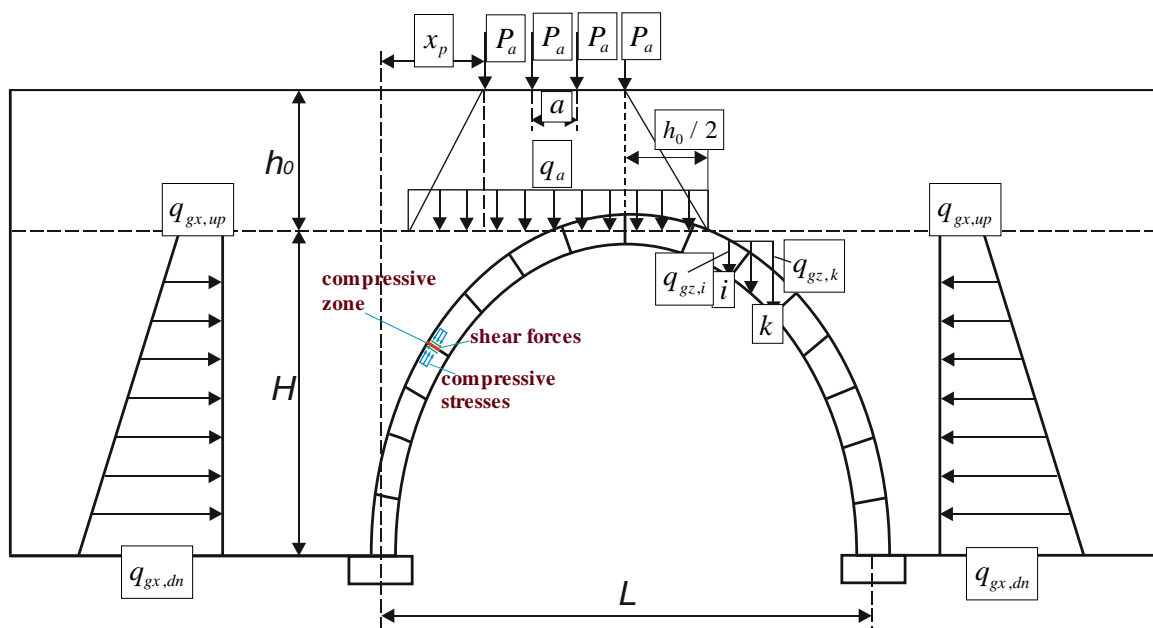


Figure 1. Loads acting on the arch.

The arch is divided lengthwise into finite elements. Bending moments and longitudinal forces are approximated along the length of each finite element by linear functions independently (Fig. 2). In Fig. 2 the unknowns numbering for the first two finite elements are shown. Due to the node equilibrium equations, under the action of a possible displacement in a rotation angle form, the equality of the moments in the nodes will be ensured.

The concrete stress-strain diagram of the arch is presented in the piecewise-broken curve form, which does not consider the tensile concrete stresses (Fig. 3). Such a diagram is used because tensile stresses cannot arise in the concrete blocks joints sections. In the sections between the joints, for the safety margin, the tensile concrete stresses will also be neglected. With this approach, the arch calculation will not depend on the length of the concrete blocks and the number of joints.

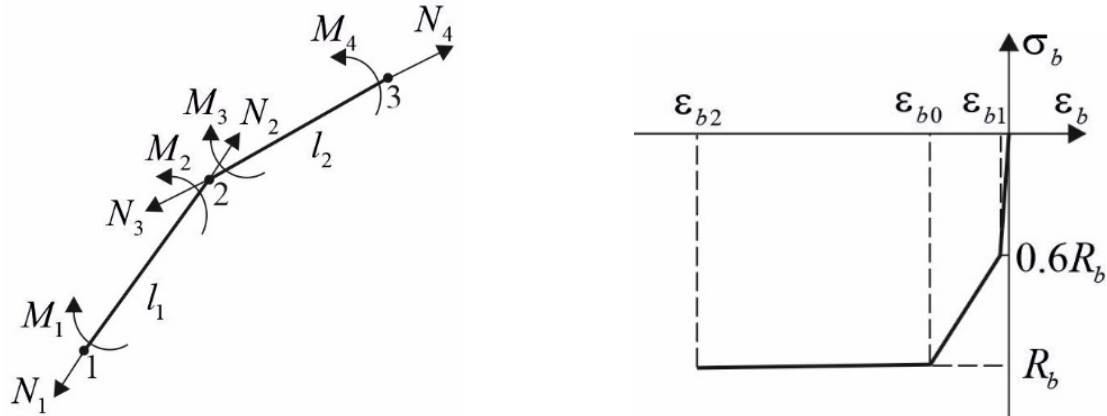


Figure 2. Numbering of the unknown nodal forces. Figure 3. Diagram of a concrete deformation.

To solve the problem with a physically nonlinear formulation, we will use the possible stress states principle. For an arbitrary step of an increasing load, variation of the additional deformation energy increment $\delta(\Delta\Pi_i)$ is zero (1).

$$\delta(\Delta\Pi_i) = \int_V (\epsilon_i + \delta(\Delta\epsilon_i)) \delta(\Delta\sigma_i) dV = 0. \quad (1)$$

$\epsilon_i, \Delta\epsilon_i$ are the current deformations and deformations increments at a loading step i ; $\Delta\sigma_i$ is the stresses increments, which must satisfy the equilibrium equations at loading step i ; V is subject area. The deformations and stresses increment at each step are interconnected by the deformation tangent modulus $E_i^t(\epsilon_i)$:

$$\Delta\sigma_i = E_i^t(\epsilon_i) \Delta\epsilon_i. \quad (2)$$

Substituting (2) into (1), we get:

$$\delta(\Delta\Pi_i) = \int_V E_i^t(\epsilon_i) (\epsilon_i + \delta(\Delta\epsilon_i)) \delta(\Delta\epsilon_i) dV = 0. \quad (3)$$

From expression (3) it follows that the additional strain energy increment will have the following form:

$$\Delta\Pi_i = \int_V \left(E_i^t(\epsilon_i) \epsilon_i \Delta\epsilon_i + \frac{1}{2} E_i^t(\epsilon_i) \Delta\epsilon_i^2 \right) dV. \quad (4)$$

Let us calculate the additional energy deformations increment of a rod finite element. The strains increments are determined according to the straight normal hypothesis:

$$\Delta\epsilon_i = \Delta\epsilon_{0i} - z\Delta\chi_i. \quad (5)$$

$\Delta\epsilon_{0i}$ is the increment of midline deformation; $\Delta\chi_i$ is axis curvature increment. Substituting (5) into (4), we get:

$$\Delta\Pi_{i,k} = \int_0^{l_k} \int_{-h/2}^{h/2} b(\varepsilon_{0i} - z\chi_i)\Delta\sigma_i dz dx + \frac{1}{2} \int_0^{l_k} \int_{-h/2}^{h/2} bE_i^t(\varepsilon_i) \left(\Delta\varepsilon_{0i}^2 - 2z\Delta\varepsilon_{0i}\Delta\chi_i + \Delta\chi_i^2 \right) dz dx. \quad (6)$$

Let us introduce notation for the following integrals:

$$EA^t = \int_{-h/2}^{h/2} bE_i^t(\varepsilon_i) dz, \quad ES^t = \int_{-h/2}^{h/2} bE_i^t(\varepsilon_i) z dz, \quad EI^t = \int_{-h/2}^{h/2} bE_i^t(\varepsilon_i) z^2 dz. \quad (7)$$

Integrals (7) are calculated numerically using the concrete stress-strain diagram (Fig. 3) by the trapezia method. Considering (7), the internal forces increment in the section are determined by the following formulas:

$$\Delta N_i = \int_{-h/2}^{h/2} b\Delta\sigma_i dz = \int_{-h/2}^{h/2} bE_i^t(\varepsilon_i) (\Delta\varepsilon_{0i} - z\Delta\chi_i) dz = \Delta\varepsilon_{0i}EA^t - \Delta\chi_{ii}ES^t, \quad (8)$$

$$\Delta M_i = - \int_{-h/2}^{h/2} b\Delta\sigma_i z dz = - \int_{-h/2}^{h/2} bE_i^t(\varepsilon_i) (z\Delta\varepsilon_{0i} - z^2\Delta\chi_i) dz = -\Delta\varepsilon_{0i}ES^t + \Delta\chi_{ii}EI^t. \quad (9)$$

From expressions (8), (9) we obtain

$$\Delta\varepsilon_{0i} = \frac{\Delta N_i EI^t + \Delta M_i ES^t}{EA^t EI^t - ES^{t2}}, \quad \Delta\chi_i = \frac{\Delta N_i ES^t + \Delta M_i EA^t}{EA^t EI^t - ES^{t2}}. \quad (10)$$

Substituting (10) into (6), we get

$$\Delta\Pi_{i,k} = \int_0^{l_k} (\varepsilon_{0i}\Delta N_i + \chi_i\Delta M_i) dx + \frac{1}{2} \int_0^{l_k} \left(\frac{EI^t \Delta N_i^2}{EI^t EA^t - ES^{t2}} + \frac{EA^t \Delta M_i^2}{EI^t EA^t - ES^{t2}} + \frac{2ES^t \Delta M_i \Delta N_i}{EI^t EA^t - ES^{t2}} \right) dx. \quad (11)$$

Let us introduce the vectors of unknown nodal forces and its increments for a finite element k :

$$\mathbf{S}_{i,k} = \begin{Bmatrix} N_{i,2k-1} \\ M_{i,2k-1} \\ N_{i,2k} \\ M_{i,2k} \end{Bmatrix}, \quad \Delta\mathbf{S}_{i,k} = \begin{Bmatrix} \Delta N_{i,2k-1} \\ \Delta M_{i,2k-1} \\ \Delta N_{i,2k} \\ \Delta M_{i,2k} \end{Bmatrix}. \quad (12)$$

To approximate the forces and moments along the finite element length, we will use linear functions. The approximations are independent for each finite element. In this case, the global flexibility matrix has a block-diagonal shape and be easily reversible. The expression (11) can be written in matrix form:

$$\Delta\Pi_{i,k} = \frac{1}{2} \Delta\mathbf{S}_{i,k}^T \mathbf{D}_{i,k}^t \Delta\mathbf{S}_{i,k} + \Delta\mathbf{L}_{i,k}^T \Delta\mathbf{S}_{i,k}, \quad (13)$$

The second integral in (11), which determines the tangent matrix elements, is calculated numerically using the trapezia formula. Divide the finite element into n equal segments $\Delta l_k = l_k / n$. Let us denote the shear stiffness generalized parameters of the section at an arbitrary point j of a finite element k :

$$EA_{k,j}^t = \int_{-h_j/2}^{h_j/2} b_j E_{k,i}^t(\varepsilon_{k,j}) dz, \quad ES_{k,j}^t = \int_{-h_j/2}^{h_j/2} b_j E_{k,i}^t(\varepsilon_{k,j}) z dz, \quad EI_{k,j}^t = \int_{-h_j/2}^{h_j/2} b_j E_{k,i}^t(\varepsilon_{k,j}) z^2 dz, \quad (14)$$

$$ER_{k,j}^t = EI_{k,j}^t EA_{k,j}^t - ES_{k,j}^{t2}.$$

b_j, h_j are the section dimensions at point j . $\varepsilon_{k,j}(z)$ is the deformation at point j :

$$\varepsilon_{k,j} = \left(\varepsilon_{i,2k-1} - z\chi_{i,2k-1} \right) \left(\frac{l_k - x_j}{l_k} \right) + \left(\varepsilon_{i,2k} - z\chi_{i,2k} \right) \left(\frac{x_j}{l_k} \right). \quad (15)$$

$\varepsilon_{i,2k-1}, \chi_{i,2k-1}, \varepsilon_{i,2k}, \chi_{i,2k}$ are deformations and curvatures of axis at the beginning and end a finite element k ; x_j is a local coordinate of point j . Let us introduce the tangent matrix $\mathbf{D}_{i,k}^t$ elements notation:

$$\begin{aligned} d_{1,1} &= \sum_{j=2}^n \frac{EI_{k,j}^t \left(1 - \frac{x_j}{l_k}\right)^2}{ER_{k,j}^t} + \frac{EI_{k,1}^t}{2ER_{k,1}^t}, d_{1,2} = \sum_{j=2}^n \frac{ES_{k,j}^t \left(1 - \frac{x_j}{l_k}\right)^2}{ER_{k,j}^t} + \frac{ES_{k,1}^t}{2ER_{k,1}^t}, d_{1,3} = \sum_{j=2}^n \frac{EI_{k,j}^t \left(1 - \frac{x_j}{l_k}\right) \frac{x_j}{l_k}}{ER_{k,j}^t}, \\ d_{1,4} &= \sum_{j=2}^n \frac{ES_{k,j}^t \left(1 - \frac{x_j}{l_k}\right) \frac{x_j}{l_k}}{ER_{k,j}^t}, d_{2,2} = \sum_{j=2}^n \frac{EA_{k,j}^t \left(1 - \frac{x_j}{l_k}\right)^2}{ER_{k,j}^t} + \frac{EA_{k,1}^t}{2ER_{k,1}^t}, d_{2,3} = d_{1,4}, d_{2,4} = \sum_{j=2}^n \frac{EA_{k,j}^t \left(1 - \frac{x_j}{l_k}\right) \frac{x_j}{l_k}}{ER_{k,j}^t}, \\ d_{3,3} &= \sum_{j=2}^n \frac{EI_{k,j}^t \left(\frac{x_j}{l_k}\right)^2}{ER_{k,j}^t} + \frac{EI_{k,n+1}^t}{2ER_{k,n+1}^t}, d_{3,4} = \sum_{j=2}^n \frac{ES_{k,j}^t \left(\frac{x_j}{l_k}\right)^2}{ER_{k,j}^t} + \frac{ES_{k,n+1}^t}{2ER_{k,n+1}^t}, d_{4,4} = \sum_{j=2}^n \frac{EA_{k,j}^t \left(\frac{x_j}{l_k}\right)^2}{ER_{k,j}^t} + \frac{EA_{k,n+1}^t}{2ER_{k,n+1}^t}. \end{aligned} \quad (16)$$

The final matrix $\mathbf{D}_{i,k}^t$ expression is as follows:

$$\mathbf{D}_{i,k}^t = \Delta l_k \begin{bmatrix} d_{1,1} & d_{1,2} & d_{1,3} & d_{1,4} \\ d_{1,2} & d_{2,2} & d_{2,3} & d_{2,4} \\ d_{1,3} & d_{2,3} & d_{3,3} & d_{3,4} \\ d_{1,4} & d_{2,4} & d_{3,4} & d_{4,4} \end{bmatrix}. \quad (17)$$

From the matrices $\mathbf{D}_{i,k}^t$ of finite elements we form the global matrix:

$$\mathbf{D}_i^t = \begin{bmatrix} \mathbf{D}_{i,1}^t & & & \\ & \mathbf{D}_{i,2}^t & & \\ & & \ddots & \\ & & & \mathbf{D}_{i,n}^t \end{bmatrix}. \quad (18)$$

Consider the linear nature of the change in forces and moments along the finite element, we obtain the expression for the vector $\Delta_{i,k}$:

$$\Delta_{i,k} = l_k \begin{Bmatrix} \frac{\varepsilon_{i,2k-1}}{3} + \frac{\varepsilon_{i,2k}}{6} \\ \frac{\chi_{i,2k-1}}{3} + \frac{\chi_{i,2k}}{6} \\ \frac{\varepsilon_{i,2k-1}}{6} + \frac{\varepsilon_{i,2k}}{3} \\ \frac{\chi_{i,2k-1}}{6} + \frac{\chi_{i,2k}}{3} \end{Bmatrix}. \quad (19)$$

Then, for the whole system, we obtain the following expression for the increment of additional energy of the deformations:

$$\Delta \Pi_i = \frac{1}{2} \Delta \mathbf{S}_i^T \mathbf{D}_i^t \Delta \mathbf{S}_i + \Delta_{i,k}^T \Delta \mathbf{S}_i. \quad (20)$$

In accordance with the possible stress states principle, the forces and moments increments must satisfy the equilibrium equations. Such equations for nodes can be obtained using the possible

displacements principle [23]. The vertical, horizontal displacements and angles rotations of nodes are taken as possible displacements. As a result, we obtain equations for the equilibrium of forces and moments for each unsecured arch node. For the whole system, the equilibrium equations can be written in the following matrix form:

$$\mathbf{L}\Delta\mathbf{S}_i + \Delta\mathbf{P}_i = 0. \quad (21)$$

The equilibrium global matrix \mathbf{L} is formed from equilibrium matrices \mathbf{L}_k of finite elements.

$$\mathbf{L}_k = \begin{bmatrix} \frac{-\cos \alpha_k}{2} & \frac{\sin \alpha_k}{l_k} & \frac{-\cos \alpha_k}{2} & \frac{-\sin \alpha_k}{l_k} \\ \frac{-\sin \alpha_k}{2} & \frac{-\cos \alpha_k}{2} & \frac{-\sin \alpha_k}{2} & \frac{\cos \alpha_k}{2} \\ 0 & 1 & 0 & 0 \\ \frac{\cos \alpha_k}{2} & \frac{-\sin \alpha_k}{l_k} & \frac{\cos \alpha_k}{2} & \frac{\sin \alpha_k}{l_k} \\ \frac{\sin \alpha_k}{2} & \frac{\cos \alpha_k}{l_k} & \frac{\sin \alpha_k}{2} & \frac{-\cos \alpha_k}{l_k} \\ 0 & 0 & 0 & -1 \end{bmatrix}, \cos \alpha_k = \frac{x_{2k} - x_{2k-1}}{l_k}, \sin \alpha_k = \frac{y_{2k} - y_{2k-1}}{l_k}. \quad (22)$$

Note that the matrix \mathbf{L} is geometric and does not depend on a load. The load vector $\Delta\mathbf{P}_i$ is formed from the forces concentrated in the nodes and the loads distributed over the finite element. For that we must calculate the load work at possible displacements of the nodes.

Using the Lagrange multiplier method, we add the nodes equilibrium equations (21) with the functional (20). We get the following advanced functional:

$$\Delta\Pi_i = \frac{1}{2}\Delta\mathbf{S}_i^T \mathbf{D}_i^t \Delta\mathbf{S}_i + \Delta_i^T \Delta\mathbf{S}_i + \mathbf{w}_i^T (\mathbf{L}\Delta\mathbf{S}_i + \Delta\mathbf{P}_i). \quad (23)$$

The Lagrange multipliers vector consists of nodal displacements and rotation angles values:

$$\mathbf{w}_i^T = (u_1 \quad w_1 \quad \varphi_1 \quad u_2 \quad w_2 \quad \varphi_2 \quad \cdots \quad \cdots \quad u_n \quad w_n \quad \varphi_n). \quad (24)$$

Equating the functional derivatives with respect to vectors $\Delta\mathbf{S}_i^T$ and \mathbf{w}_i^T , we obtain the linear algebraic equations system:

$$\begin{aligned} \mathbf{D}_i^t \Delta\mathbf{S}_i + \Delta_i + \mathbf{L}^T \mathbf{w}_i &= 0, \\ \mathbf{L}\Delta\mathbf{S}_i + \Delta\mathbf{P}_i &= 0. \end{aligned} \quad (25)$$

Let us express from the first equation the forces increment vector

$$\Delta\mathbf{S}_i = -\mathbf{D}_i^{t-1} \Delta_i - \mathbf{D}_i^{t-1} \mathbf{L}^T \mathbf{w}_i. \quad (26)$$

The matrix \mathbf{D}_i^t is block-diagonal and easily inverted. Let us introduce notation of the matrix product:

$$\mathbf{K}_i = \mathbf{L}\mathbf{D}_i^{t-1} \mathbf{L}^T. \quad (27)$$

From the second equation (25) we obtain the resolving system of nonlinear algebraic equations

$$\mathbf{K}_i \mathbf{w}_i = \Delta\mathbf{P}_i - \mathbf{L}\mathbf{D}_i^{t-1} \Delta_i. \quad (28)$$

For solving (28), we will perform iterative refinement according to the Newton - Raphson scheme. We will use the following calculation algorithm with given automobile position:

1. Calculate matrix \mathbf{L} and vector \mathbf{P} ; $\mathbf{S}_0 = 0$; for each node k : $\varepsilon_{0,k} = 0$, $\chi_{0,k} = 0$.

2. Accept $\Delta \mathbf{P}_i = \mathbf{P}$, $i=0$.
3. Begin cycle of iterative refinement; accept $i = i + 1$.
4. Calculate matrices \mathbf{D}_i^t , \mathbf{D}_i^{t-1} , \mathbf{K} , Δ_i .
5. Calculating equations system (28), we get \mathbf{w}_i .
6. Using (26), we calculate $\Delta \mathbf{S}_i$.
7. Using (10), we calculate for all nodes: $\Delta \varepsilon_{i,k}$, $\Delta \chi_{i,k}$;
8. Calculate for all nodes $\varepsilon_{i,k} = \varepsilon_{i-1,k} + \Delta \varepsilon_{i,k}$, $\chi_{i,k} = \chi_{i-1,k} + \Delta \chi_{i,k}$.
9. Using in (8) and (9) the secant modulus of deformations we calculate $\bar{\mathbf{S}}_i$.
10. Calculate $\Delta \bar{\mathbf{S}}_i = \mathbf{S}_{i-1} - \bar{\mathbf{S}}_i$.
11. Calculate $\Delta \bar{\mathbf{P}}_i = \mathbf{L} \Delta \bar{\mathbf{S}}_i$ and accuracy $Ex(\Delta \mathbf{P}_i) = 100 \frac{\sqrt{\sum_{j=1}^{n_d} (P_{i,j} - \Delta \bar{P}_{i,j})^2}}{\sqrt{\sum_{j=1}^{n_d} P_{i,j}^2}}$.
12. If $Ex(\Delta \mathbf{P}_i) > [Ex]$, then we calculate $\Delta \mathbf{P}_i = \mathbf{P}_i - \mathbf{L} \Delta \bar{\mathbf{S}}_i$; $\mathbf{S}_i = \bar{\mathbf{S}}_i$ and go to 3.
13. If $Ex(\Delta \mathbf{P}_i) \leq [Ex]$, then we have end of iterative refinement.

The resulting bending moments are used to calculate the shear forces in finite elements:

$$Q_k = \frac{M_{2k} - M_{2k-1}}{l_k}. \quad (29)$$

Next, a check is carried out for a possible displacement of the sections at the joints of concrete blocks:

$$|Q_k| \leq k_{fr} |N_{2k-1}|, \quad |Q_k| \leq k_{fr} |N_{2k}|. \quad (30)$$

k_{fr} is the friction coefficient of concrete on concrete; $N_{2k-1}, M_{2k-1}, N_{2k}, M_{2k}$ are the internal forces at the finite element beginning and end. If conditions (30) are not done, then a shift of concrete blocks relative to each other is possible and it is necessary to change a design scheme.

At each node of the arch, the eccentricity modulus of the longitudinal force and the required section height are calculated, which provides the compressed zone will be equal to half the section height (with a linear stress diagram in the compressed zone):

$$e_i = \left| \frac{M_i}{N_i} \right|, \quad h_i^s = 3 \cdot e_i. \quad (31)$$

Calculations have shown that the maximum compressive stresses are far from the limiting value; therefore, the stress diagram in the compressed zone is practically linear. Nonlinearity of deformations is associated with the exclusion of the stretched concrete zone from the work.

The required heights of the arch cross sections will be determined using the following iterative algorithm:

1. For each arch node i , we set the initial value of the section height $h_i = h_{\min}$.
2. Begin cycle of h_i finding.
3. Set $h_i^{iter} = h_i$.

4. Begin cycle on x_p (Fig.1) from 0 to $\left(\frac{L}{2} - \frac{a_x}{2}\right)$ with step 0.1 m.
5. We perform the arch calculation according to the algorithm given above.
6. For each arch node, we calculate h_i^s (31).
7. If $h_i^s > h_i^{iter}$, then $h_i^{iter} = h_i^s$.
8. End cycle on x_p .
9. For each arch node i , we calculate $h_i = \left(\frac{10000 \cdot h_i^{iter} + h_i}{10000}\right) \geq h_{\min}$.
10. Rounding h_i to 5 cm.
11. Go to 3.

The calculations have shown that the process of refining the cross-section heights converges in no more than 15 iterations. As a result of the calculation, for each node, the maximum eccentricities of the longitudinal force and the required section height are determined. These heights will ensure the compressed zone value at least half of the cross section at any automobile load position.

3. Results and Discussion

Consider the problem of determining the optimal parameters of an elliptical arch bridge. The arch is subject to loads from the weight of the backfill soil and a load from the moving vehicle (Fig. 1). In this case, the compressed zone minimum height should be at least half the arch section height. When searching for the optimal parameters, we will assume that the arch span L is given, and the optimal arch height H must be selected. The optimal height is determined by sequential calculation of the arches with it gradual increasing. The all data for the calculation are given in Table 1. The arch was divided along the length into 16 finite elements.

Table 1. Arch calculation data.

Denotation	Dimension	Value	Parameter
h_0	m	2.0	Backfill height from the arch top
φ_{gr}	degree	35	Angle of internal soil friction
γ_{gr}	kN/m ³	17.7	Soil volume weight
a	m	1.2	Distance between vehicle axles
P_a	kN	250	Vehicle axle load
a_x	m	3.6	Load length from vehicle
a_y	m	2.7	Load width from vehicle
L	m	12	Arch span
B	m	0.5	Arch width is a bridge strip width on which the load is collected
h_{\min}	m	Need to assign	The minimum height of the arch cross section
H	m	Need to define	Arch height

Vertical and horizontal loads from the vehicle and the ground (Fig. 1) are determined by the following formulas:

$$q_a = \frac{1.2 \cdot B \cdot P_a}{(h_0 + a_x)(h_0 + a_y)}, q_{gz,i} = 1.1 \cdot \gamma_{gr} (H + h_0 - z_i) \cdot B. \quad (32)$$

$$q_{qx,up} = 1.1 \cdot \gamma_{gr} h_0 \cdot tg^2 \left(45 - \frac{\varphi_{gr}}{2} \right) B, q_{qx,dn} = 1.1 \cdot \gamma_{gr} (H + h_0) \cdot tg^2 \left(45 - \frac{\varphi_{gr}}{2} \right) B. \quad (33)$$

To these loads is added the load from the arch own weight.

The parameters of the compressed concrete deformation diagram were taken as follows: $\varepsilon_{b1} = -0.000314$, $\varepsilon_{b0} = -0.002$, $\varepsilon_{b2} = -0.0035$, $R_b = 17000 \text{ kN} / \text{m}^2$ (Fig. 2).

Fig. 4 shows the most optimal arch minimum weight ($h_{\min} = 0.4 \text{ m}$).

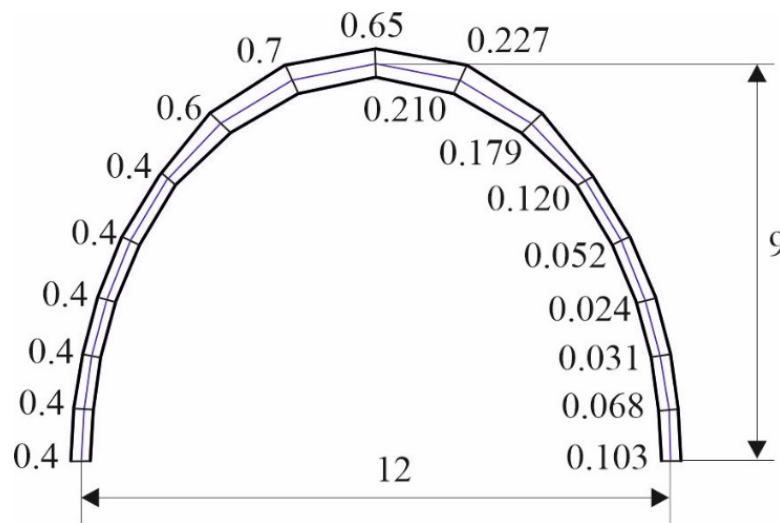


Figure 4. Arch with minimum weight of 15.409 tons: on the left side the blocks section heights are indicated; on the right side the maximum eccentricities of the longitudinal force (in meters) are indicated.

The arch division into finite elements was carried out automatically. Arch nodes were defined as the point of intersection of a straight line drawn from the span middle and an elliptical arc. Straight lines were drawn with an angular step of 11.25 degrees. The angles were measured from the horizontal line. The first five finite elements of half-arch have a minimum cross-section height. Further, an increase of the section height is required to 0.6–0.7 meters.

Table 2. Arch weight (tons) depending on geometric parameters.

H [m]	h_{\min} [m]		
	0.4	0.5	0.6
8.8	-	17.471	18.534
8.9	15.498	16.690	18.668
9.0	15.409	16.816	18.802
9.1	15.761	17.175	18.936
9.2	16.001	17.536	19.308

Table 2 shows optimal weights of arches, depending on an arch height and a specified minimum section height. Note that the arch optimal weight is more influenced by a value of minimum section height, which is specified. Setting a minimum arch height is necessary to meet possible construction requirements. Also note that the greater a minimum section height, the lower an optimal arch height.

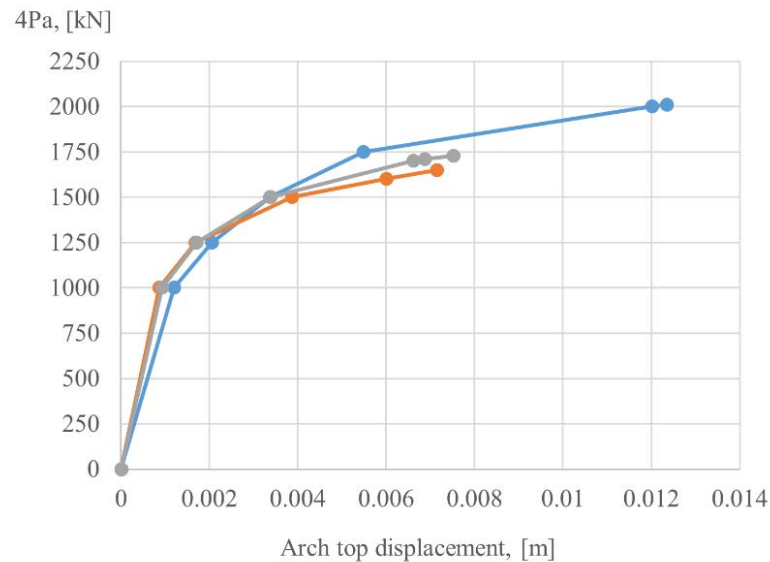


Figure 5. The arch top displacements depending on the Vehicle axle load value. Blue line – the load is located symmetrically from the center; gray line – the load is displaced on 1.2 meters from the center; red line – the load is displaced on 2.4 meters from the center.

Also, to determine the bearing capacity reserve of the optimal arch, the arch calculations were performed with a gradual increase in the automobile load up to destruction. Three options for the vehicle load location were considered (Fig. 5). The most dangerous is the load location with an offset of 2.4 meters from the top of the arch (red line in Fig. 5). In this case, the ultimate automobile load is approximately 1.6 times higher than the calculated one. This value shows the safety margin of the arch. The danger of an asymmetrical arrangement of the load for arches made of stone blocks is also noted in [1, 4]. If the vehicle load is located symmetrically with respect to the arch top, then the breaking load value is twice the calculated one. If it is necessary to provide a greater safety margin for the arch, then we must take the minimum height of the compressed zone more than half the section height. The arch, which is optimal in terms of weight, has a cross section that is variable in length, so concrete blocks must be manufactured individually. Also, the blocks must have the required slope of the faces to ensure the compressive forces transmission. For the manufacture of such blocks, it is necessary to have a steel mold with three moving faces, which is quite technically feasible and will not lead to a significant blocks cost increase. At the same time, by reducing the concrete arch volume, the building materials cost is can reduced significant. If necessary, you can determine the arch optimal height with a constant section size, but such an arch will not have a minimum weight. For example, the arch in Fig. 4 with the constant maximum required section height of 0.7 meters will have a weight of approximately 22 tons, which is 1.5 times more than the optimal one.

4. Conclusions

1. An algorithm for determining the optimal parameters of an elliptical arched road bridge made of concrete blocks is proposed. With a given bridge span and a given minimum section height, the arch height and the section height change along the length are determined, providing the minimum arch weight under the design loads action.

2. The solution of a physically nonlinear problem is based on the principles of possible stress states and possible displacements. Internal forces are approximated by linear functions, the concrete deformation diagram is represented as a piecewise broken curve.

3. The optimal parameters of an arched road bridge with a span of 12 meters and its bearing capacity have been determined. It is shown that the arch destruction occurs with an increase in the automobile load by about 1.6 times, what shows the safety margin of the arch. This arch with the constant maximum required section height of 0.7 meters will have a weight of approximately 22 tons, which is 1.5 times more than the optimal one.

References

1. AudioNet, A., Fanning, P., Sobczak, L., Peremans, H. 2-D analysis of arch bridges using an elasto-plastic material model. *Engineering Structures*. 2008. 30(3). Pp. 845–855. DOI:10.1016/j.engstruct.2007.05.018.
2. Amorim, D.L.N.D.F., Proença, S.P.B., Flórez-López, J. A model of fracture in reinforced concrete arches based on lumped damage mechanics. *International Journal of Solids and Structures*. 2013. 50(24). Pp. 4070–4079. DOI:10.1016/j.ijsolstr.2013.08.012.

3. Galassi, S., Misseri, G., Rovero, L., Tempesta, G. Failure modes prediction of masonry voussoir arches on moving supports. *Engineering Structures*. 2018. 173. Pp. 706–717. DOI:10.1016/j.engstruct.2018.07.015.
4. Gattesco, N., Boem, I., Andretta, V. Experimental behaviour of non-structural masonry vaults reinforced through fibre-reinforced mortar coating and subjected to cyclic horizontal loads. *Engineering Structures*. 2018. 172. Pp. 419–431. DOI:10.1016/j.engstruct.2018.06.044.
5. Beatini, V., Royer-Carfagni, G., Tasora, A. Modeling the shear failure of segmental arches. *International Journal of Solids and Structures*. 2019. 158. Pp. 21–39. DOI:10.1016/j.ijsolstr.2018.08.023.
6. Houšť, V., Eliáš, J., Miča, L. Shape optimization of concrete buried arches. *Engineering Structures*. 2013. 48. Pp. 716–726. DOI:10.1016/j.engstruct.2012.11.037.
7. Kimura, T., Ohsaki, M., Fujita, S., Michiels, T., Adriaenssens, S. Shape optimization of no-tension arches subjected to in-plane loading. *Structures*. 2020. 28. Pp. 158–169. DOI:10.1016/j.istruc.2020.08.053.
8. Misseri, G., Justin, M., Rovero, L. Experimental and numerical investigation of the collapse of pointed masonry arches under quasi-static horizontal loading. *Engineering Structures*. 2018. 173. Pp. 180–190. DOI:10.1016/j.engstruct.2018.06.009.
9. Pulatsu, B., Erdogmus, E., Lourenço, P.B. Comparison of in-plane and out-of-plane failure modes of masonry arch bridges using discontinuum analysis. *Engineering Structures*. 2019. 178. Pp. 24–36. DOI:10.1016/j.engstruct.2018.10.016.
10. Scozzese, F., Ragni, L., Tubaldi, E., Gara, F. Modal properties variation and collapse assessment of masonry arch bridges under scour action. *Engineering Structures*. 2019. 199. Pp. 109665. DOI:10.1016/j.engstruct.2019.109665.
11. Smoljanović, H., Živaljić, N., Nikolić, Ž., Munjiza, A. Numerical analysis of 3D dry-stone masonry structures by combined finite-discrete element method. *International Journal of Solids and Structures*. 2018. 136–137. Pp. 150–167. DOI:10.1016/j.ijsolstr.2017.12.012.
12. Zampieri, P., Simoncello, N., Tetougueni, C.D., Pellegrino, C. Review article A review of methods for strengthening of masonry arches with composite materials. *Engineering Structures*. 2018. 171. Pp. 154–169. DOI:10.1016/j.engstruct.2018.05.070.
13. Zampieri, P., Simoncello, N., Gonzalez-libreros, J., Pellegrino, C. Evaluation of the vertical load capacity of masonry arch bridges strengthened with FRCM or SFRM by limit analysis. *Engineering Structures*. 2020. 225. 111135. DOI:10.1016/j.engstruct.2020.111135.
14. Dmitriev, A., Lalin, V., Novozhilov, Y., Mikhalyuk, D. Simulation of Concrete Plate Perforation by Coupled Structures. 2020. 92(9207). DOI:10.18720/CUBS.92.7.
15. Ribeiro, F., Sena-Cruz, J., Branco, F.G., Júlio, E. 3D finite element model for hybrid FRP-confined concrete in compression using modified CDPM. *Engineering Structures*. 2019. 190. Pp. 459–479. DOI:10.1016/j.engstruct.2019.04.027.
16. Zani, G., Martinelli, P., Galli, A., di Prisco, M. Three-dimensional modelling of a multi-span masonry arch bridge: Influence of soil compressibility on the structural response under vertical static loads. *Engineering Structures*. 2020. 221. 110998. DOI:10.1016/j.engstruct.2020.110998.
17. Zhao, C., Xiong, Y., Zhong, X., Shi, Z., Yang, S. A two-phase modeling strategy for analyzing the failure process of masonry arches. *Engineering Structures*. 2020. 212. Pp. 110525. DOI:10.1016/j.engstruct.2020.110525.
18. Mohireva, A., Proskurovskis, A., Belousov, N., Nazinyan, A., Glebova, E. Strength and deformability of compressed-bent masonry structures during and after fire. *Construction of Unique Buildings and Structures*. 2020. 92(9203). Pp. 2–6. DOI:10.18720/CUBS.92.3.
19. Thai, S., Thai, H.T., Vo, T.P., Patel, V.I. A simple shear deformation theory for nonlocal beams. *Composite Structures*. 2016. 183(1). Pp. 262–270. DOI:10.1016/j.compstruct.2017.03.022.
20. Pydah, A., Batra, R.C. Shear deformation theory using logarithmic function for thick circular beams and analytical solution for bi-directional functionally graded circular beams. *Composite Structures*. 2017. 172. Pp. 45–60. DOI:10.1016/j.compstruct.2017.03.072.
21. Tyukalov, Y.Y. Optimal Shape of Arch Concrete Block Bridge. *Construction of Unique Buildings and Structures*. 2020. 93. 9307. DOI: 10.18720/CUBS.93.7
22. Tyukalov, Y.Y. Calculation of circular plates with assuming shear deformations. *IOP Conference Series: Materials Science and Engineering*. 2019. 687(3). DOI: 10.1088/1757-899X/687/3/033004.
23. Tyukalov, Y.Y. Calculation of bending plates by finite element method in stresses. *IOP Conference Series: Materials Science and Engineering*. 2018. 451(1). DOI: 10.1088/1757-899X/451/1/012046.
24. Cannizzaro, F., Pantò, B., Caddemi, S., Calì, I. A Discrete Macro-Element Method (DMEM) for the nonlinear structural assessment of masonry arches. *Engineering Structures*. 2018. 168. Pp. 243–256. DOI: 10.1016/j.engstruct.2018.04.006.
25. Mahmoudi Moazam, A., Hasani, N., Yazdani, M. Incremental dynamic analysis of small to medium spans plain concrete arch bridges. *Engineering Failure Analysis*, 2018. 91. Pp. 12–27. DOI: 10.1016/j.engfailanal.2018.04.027.
26. Pulatsu, B., Erdogmus, E., Bretas, E. M. Parametric Study on Masonry Arches Using 2D Discrete-Element Modeling. *Journal of Architectural Engineering*. 2018. 24(2). 04018005. DOI:10.1061/(asce)ae.1943-5568.0000305.
27. Zhang, Y., Tubaldi, E., Macorini, L., Izzuddin, B. A. Mesoscale partitioned modelling of masonry bridges allowing for arch-backfill interaction. *Construction and Building Materials*. 2018. 173. Pp. 820–842. DOI: 10.1016/j.conbuildmat.2018.03.272.
28. Fusade, L., Orr, S. A., Wood, C., O'Dowd, M., Viles, H. (2019). Drying response of lime-mortar joints in granite masonry after an intense rainfall and after repointing. *Heritage Science*. 2019. 7(1). DOI: 10.1186/s40494-019-0277-7.
29. Leontari, A., Apostolou, M. Stability and rocking response of non-uniform masonry arches: The 'part-elliptical' profile. *Engineering Structures*. 2021. 228. DOI:10.1016/j.engstruct.2020.111519.
30. Grosman, S., Bilbao, A. B., Macorini, L., Izzuddin, B. A. Numerical modelling of three-dimensional masonry arch bridge structures. *Proceedings of the Institution of Civil Engineers - Engineering and Computational Mechanics*. 2021. 174(2). Pp. 96–113. DOI:10.1680/jenm.20.00028.

Information about authors:

Yury Tyukalov, Doctor of Technical Science

ORCID: <https://orcid.org/0000-0001-6184-2365>

E-mail: yutvgu@mail.ru

Received 25.05.2021. Approved after reviewing 03.11.2023. Accepted 03.11.2022.